

# Gallium self-interstitial relaxation in Gallium Arsenide: an *ab initio* characterization

Marc-André Malouin,\* Fedwa El-Mellouhi,† and Normand Mousseau‡

Département de physique and Regroupement québécois sur les matériaux de pointe,  
Université de Montréal, C.P. 6128, succursale Centre-ville, Montréal (Québec) H3C 3J7, Canada

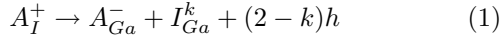
(Dated: May 5, 2022)

Ga interstitials in GaAs ( $I_{Ga}$ ) are studied using the local-orbital *ab-initio* code SIESTA in a supercell of 216+1 atoms. Starting from eight different initial configurations, we find five metastable structures: the two tetrahedral sites in addition to the 110-split<sub>[Ga-As]</sub>, 111-split<sub>[Ga-As]</sub>, and 100-split<sub>[Ga-Ga]</sub>. Studying the competition between various configuration and charges of  $I_{Ga}$  at  $T = 0$  K, we find that predominant gallium interstitials in GaAs are charged +1, neutral or at most -1 depending on doping conditions and prefer to occupy the tetrahedral configuration where it is surrounded by Ga atoms. Our results are in excellent agreement with recent experimental results concerning the dominant charge of  $I_{Ga}$ , underlining the importance of finite size effects in the calculation of defects.

PACS numbers: 61.72.Ji, 71.15.Mb, 71.15.Pd,

## I. INTRODUCTION

Gallium self-interstitials are believed to play a significant role for dopant diffusion in GaAs. The in-diffusion of an acceptor dopant  $A_I^+$  (at an interstitial position) occurs via a kick-out mechanism that transforms it to a substitutional atom ( $A_{Ga}^-$ ) and a gallium interstitial ( $I_{Ga}^k$ ) plus the emission of a number of holes (equation from cited Ref. 1):



where  $k$  denotes the charge state of  $I_{Ga}^k$  involved in the reaction.

Early calculations for Ga self-interstitials in GaAs<sup>2,3</sup> led experimental groups to propose contradicting conclusions regarding the charge state of active self-interstitials in GaAs. The suggested states varied from neutral<sup>4</sup>, to +1<sup>5,6,7</sup>, +2<sup>8,9,10</sup>, or both +2 and +3<sup>11,12</sup>. Recently, however, Bracht *et al.*<sup>1</sup> found that fits of recent as well as earlier diffusivity profiles are more accurate for dominant neutral and +1 charge states. This analysis of published data is confirmed by the observed compatibilities between the hole concentration measurements and dopant (Zn) concentrations<sup>1</sup>.

These experimental results demonstrate the need for a set of more detailed and accurate quantum mechanical calculations regarding the dominant charge state and geometry of  $I_{Ga}$  in GaAs. Most recent papers only treat a subgroup of the charge states and interstitial positions<sup>13,14</sup>, however, and we still lack a complete description of the competition between different Ga self-interstitials in GaAs. This paper intends to fill this gap by providing a unified analysis of all charge states from  $q = -3$  to  $q = +3$  for a wide range of the Ga self-interstitial configurations at  $T = 0$  K, in order to identify the dominant defects but also characterize others that could play a role in the diffusion of  $I_{Ga}$  or after ion beam implantation, for example.

This paper is organized as follows. Section II explains the methodology used for defect calculation. Next, we

describe in Section III the Gallium interstitial configurations used as starting points for this work. Section IV is devoted to study the stability of the chosen gallium interstitials after full relaxation of both the neutral and the charged states. The most relevant Ga interstitial configurations and charge states in GaAs are then deduced and compared with earlier results in Section V.

## II. METHODOLOGY

All calculations are performed using the SIESTA code<sup>15,16</sup> within density functional theory (DFT) in local-density approximation (LDA). The details of the procedure followed is discussed in our previous work<sup>17</sup> and we focus below on the operations and parameters specific to the Ga self-interstitial simulations.

### A. Simulation parameters

Simulations are performed using a supercell with 216+1 atoms. This size is just sufficient to prevent size effects from dominating the structure and energetics of defects in GaAs. The wavefunctions are constructed from a double- $\zeta$  polarized basis set (DZP) and we use a  $2 \times 2 \times 2$  Monkhorst-Pack mesh sampling<sup>17</sup>. The choice of these parameters is discussed at length in our earlier work and the reader is referred to Ref. 17 for more details.

To test the validity of the local basis set used in this work, we evaluate the heat of formation of bulk GaAs crystal ( $\Delta H$ ), defined as :

$$\Delta H = \mu_{As}^{bulk} + \mu_{Ga}^{bulk} - \mu_{GaAs}^{bulk} \quad (2)$$

For this, it is necessary to compute the *bulk* chemical potentials, calculated from a 32 atoms As lattice ( $\mu_{As}^{bulk}$ ), a 64 atoms Ga lattice ( $\mu_{Ga}^{bulk}$ ), and a 216 atoms GaAs lattice ( $\mu_{GaAs}^{bulk}$ ) respectively. The heat of formation represents the energy necessary to dissociate the GaAs crystal into its Ga and As components. Table I compares the

chemical potentials obtained using DZP with chemical potentials derived from a plane wave basis set calculation (PW) within the DFT-LDA carried out by Zollo *et al.*<sup>18</sup> on 64+1 atoms supercell. Our calculations provide an excellent agreement with experiment: both for the lattice parameter and the formation enthalpy.

TABLE I: Comparison between DFT-LDA calculations — with double- $\zeta$  polarized basis set (DZP) from this work and plane waves basis set (PW) from the work of Zollo *et al.*<sup>18</sup> — and experiment for the lattice parameter ( $\mathbf{a}$ ), chemical potentials ( $\mu$ ) and the resulting formation enthalpy ( $\Delta H$ ). *Ab-initio* calculations are performed at 0 K and experimental data at 300 K.

	DZP	PW <sup>18</sup>	Expt. <sup>19</sup>
$\mathbf{a}$ (Å)	5.60	5.55	5.65
$\mu_{Ga}^{bulk}$ (eV)	-61.487	-61.785	
$\mu_{As}^{bulk}$ (eV)	-173.83	-173.75	
$\mu_{GaAs}^{bulk}$ (eV)	-236.05	-236.12	
$\Delta H$ (eV)	-0.737	-0.985	-0.736

## B. Formation energy calculations

Ga self-interstitials are placed at various sites in the supercell. Since these positions do not necessarily correspond to a local minimum, the network is slightly distorted and the configuration is relaxed at  $T = 0$  K until a total force threshold of  $0.04$  eV/Å is reached.

The formation energy ( $E_f$ ) of each self-interstitial is calculated using

$$E_f = E'_f + q(E_V + \mu_e) - \frac{1}{2}(n_{As} - n_{Ga})\Delta\mu \quad (3)$$

where  $E'_f$  is the formation energy independent from doping and growing conditions, the next term on the right-hand side depends on the doping of the sample  $\mu_e$  (i.e. Fermi level), the charge state of the defect  $q$  and the position of the valence band maximum,  $E_V$ ; the last term is associated with the stoichiometry of the supercell containing  $n_{As}$  Arsenic and  $n_{Ga}$  Gallium atoms. Finally, the chemical potential difference  $\Delta\mu$  is defined as:

$$\Delta\mu = (\mu_{As} - \mu_{Ga}) - (\mu_{As}^{bulk} - \mu_{Ga}^{bulk}), \quad (4)$$

The independent formation energy can thus be calculated numerically using the relation:

$$E'_f = E_{tot}(q) - \frac{1}{2}(n_{As} + n_{Ga})\mu_{GaAs}^{bulk} - \frac{1}{2}(n_{As} - n_{Ga})(\mu_{As}^{bulk} - \mu_{Ga}^{bulk}) \quad (5)$$

where  $E_{tot}(q)$  correspond to the total energy of the relaxed supercell containing the self-interstitial.

The total energy of the relaxed supercell must be corrected for the strong perturbation produced by the net charge on the relaxed state symmetry and local electronic properties of the supercell. We can account for the electrostatic interaction between the charged defect and its periodic images by adding a neutralizing *jellium* background then correcting the relaxed energy ( $E_{tot}(q)$ ). Madelung correction due to the periodic boundary conditions is introduced following the Makov and Payne approximate procedure<sup>20</sup>. According to our previous work<sup>17</sup> the monopole-monopole interactions correction is calculated to be 0.094 eV, 0.37 eV, and 0.84 eV for charge states  $\pm 1$ ,  $\pm 2$ , and  $\pm 3$  respectively, while higher order corrections were found to be negligible. Charged state formation energies, from Section IV A and later, were adjusted using these corrections.

Finally, the position of the Fermi level  $\mu_e$  varies with doping and temperature and depends strongly on the carrier concentration. Thus, majority carriers (electrons or holes) can get trapped at defect levels changing the charge state of a given defect from  $q_1$  to  $q_2$ . The thermal ionization energy from a charge  $q_1$  to  $q_2$  is by definition the value of the Fermi level where the transition occurs:

$$E_{q_1/q_2} = \frac{E_{tot}(q_2) - E_{tot}(q_1) - (q_1 - q_2)E_V}{|q_1 - q_2|} \quad (6)$$

We use Eq. 6 in Section IV C to calculate ionization energies of charged defects for metastable configurations.

## III. INITIAL CONFIGURATIONS FOR THE GA INTERSTITIAL

We first determine the metastable configurations for the Ga interstitial ( $I_{Ga}$ ) with different charge states. We start in each of eight positions, relaxing the interstitial and characterizing the local energy minimum reached. All the initial states are shown on the top row of Fig. 1. The first starting point, from the left, tetra<sub>[Ga-As]</sub>, has the Ga interstitial placed in a tetrahedral position with four surrounding lattice As atoms. For the second starting configuration, tetra<sub>[Ga-Ga]</sub>, the  $I_{Ga}$  is shifted in a tetrahedral position with respect to 4 Ga atoms. In these two initial states, the bonds between the interstitial atom and its four tetrahedral neighbors, positioned on a perfect tetrahedron, have the same length of 2.425 Å, which is exactly the length of Ga-As bonds in the zincblende structure corresponding to the lattice parameter we use  $a = 5.60$  Å (see Table I).

The third starting point is an *hexagonal* interstitial configuration (hexag), where  $I_{Ga}$  is located at the center of the six-membered ring with alternating chemical species at equal distances from its six nearest neighbors. The  $I_{Ga}$ -Ga and  $I_{Ga}$ -As bond lengths are 2.322 Å while  $I_{Ga}$ -Ga-As angles all have the same value of 63.0°. We also examined a *bond-center* configuration in which  $I_{Ga}$  is lying exactly in the middle of a Ga-As bond at 1.213 Å from each of them.

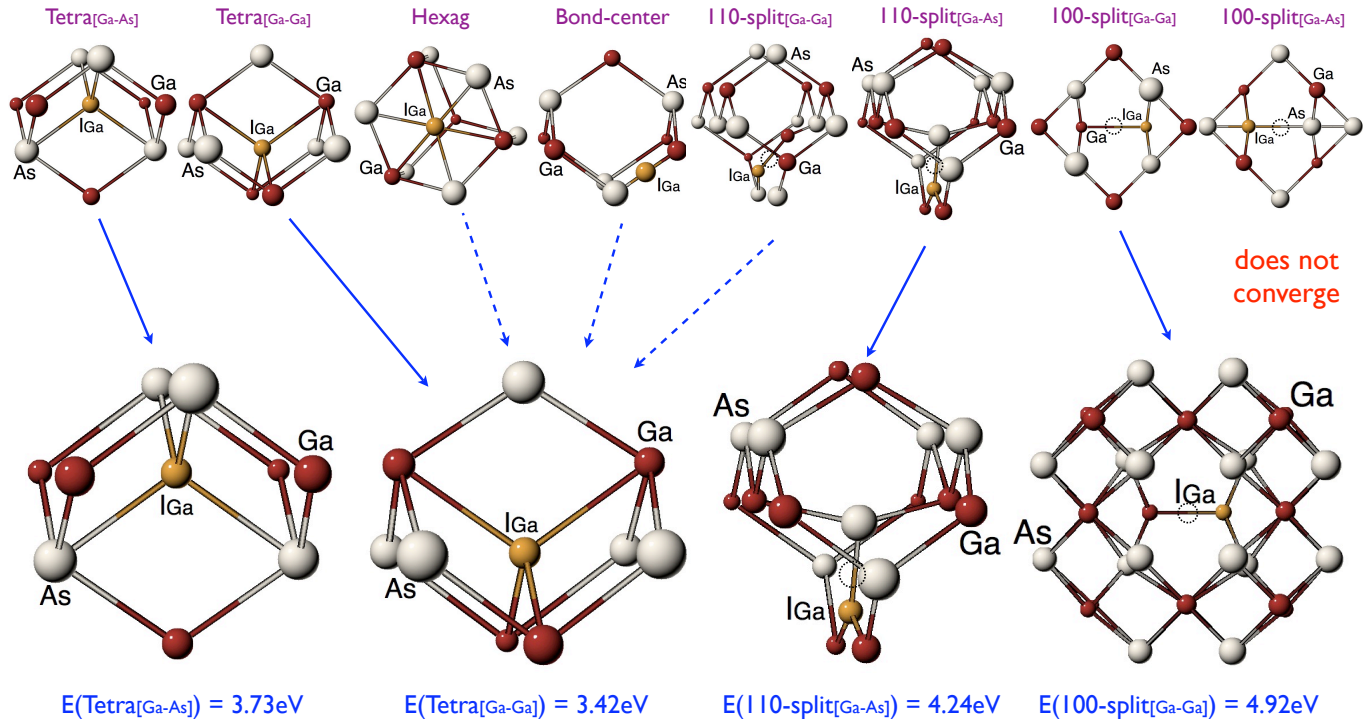


FIG. 1: (Color online) Top: The eight initial configurations considered in this study for neutral self-interstitial  $I_{Ga}$ . The six first configurations, going from left to right, are viewed near the  $\langle 110 \rangle$  direction, while the remaining two are viewed along the  $\langle 100 \rangle$  direction. Bottom: The metastable configurations obtained after full relaxation of  $I_{Ga}$ . Full arrows connect the initial configuration to its metastable counterpart, while dashed arrows means that the initial configuration is unstable and converged to the pointed configuration. Gallium atoms are red while arsenics are white; the interstitial Ga atom is colored yellow. For splits, regular sites of the displaced lattice atoms are highlighted by a dotted circle.

Finally, we look at four different interstitials from the important family of *split* geometries. Split interstitials are formed when  $I_{Ga}$  pushes one regular lattice atom (Ga or As) out of its crystalline position, forming a dumbbell centered at a regular lattice site. The split-interstitial type is determined by the orientation of the vector joining the pair of atoms (see Ref. 21). Gallium interstitials can form dumbbells with As and Ga atoms following the  $\langle 100 \rangle$  and  $\langle 110 \rangle$  directions, as shown in the top part of Fig. 1, or the  $\langle 111 \rangle$  direction.

In more details, in the  $110\text{-split}_{[\text{Ga-As}]}$  interstitial, an arsenic atom is moved by  $1.570 \text{ \AA}$  from its regular lattice site to make room for the interstitial atom positioned at  $0.840 \text{ \AA}$  from the regular lattice site and forming a dumbbell length of about  $2.312 \text{ \AA}$  along the  $\langle 110 \rangle$  direction. In this case, the center the dumbbell is slightly displaced from regular lattice site (as clearly seen in Fig. 2(a)).

For  $110\text{-split}_{[\text{Ga-Ga}]}$ , a lattice Ga atom is moved by  $1.338 \text{ \AA}$  from its lattice site along the dumbbell axis (in another  $\langle 110 \rangle$  direction) and the interstitial is placed at  $0.641 \text{ \AA}$  in the opposite direction along this axis from the lattice site. The dumbbell length is now  $1.980 \text{ \AA}$ .

For  $100\text{-split}_{[\text{Ga-Ga}]}$  and  $100\text{-split}_{[\text{Ga-As}]}$  interstitials, the lattice atom (Ga and As respectively) is moved along the dumbbell axis from its regular position by  $1.212 \text{ \AA}$  while the interstitial is placed at the same distance in the opposite direction along the same axis, forming a dumbbell of  $2.425 \text{ \AA}$ .

Other possible configurations including interstitial clusters might exist in real crystals. As a first step, we restricted ourselves to these simplest structures.

#### IV. RESULTS

Here we present the results of our simulations, using the techniques and parameters described in Section II. We first discuss the stability of the eight interstitial positions described in Section III in the neutral state. Then, we focus on the influence of the charge state on the metastable interstitial positions identified earlier. Finally, we discuss the impact of the progressive doping of the material on the competition between various charge states of a given interstitial in stoichiometric

GaAs ( $\Delta\mu = 0$ ).

### A. Structural stability of neutral self-interstitials

The bottom part of Fig. 1 shows the final geometry of the relaxed interstitial configurations in the neutral state. The most stable interstitial is the  $\text{tetra}_{[\text{Ga}-\text{Ga}]}$ , which undergoes small lattice distortions leading to its convergence into a metastable configuration with a formation energy of approximately 3.42 eV. The hexag, bond-center and 110-split $_{[\text{Ga}-\text{Ga}]}$  configurations are unstable and relax to the same  $\text{tetra}_{[\text{Ga}-\text{Ga}]}$  after undergoing considerable atomic displacement and lattice relaxation.

The second tetrahedral configuration,  $\text{tetra}_{[\text{Ga}-\text{As}]}$ , is also metastable, with a formation energy of about 3.73 eV, slightly above that of  $\text{tetra}_{[\text{Ga}-\text{As}]}$ . This structure is only a few relaxation steps away from the initial  $\text{tetra}_{[\text{Ga}-\text{As}]}$ . Both tetrahedral interstitials leave the surrounding crystalline network relatively unaffected. The  $\text{tetra}_{[\text{Ga}-\text{Ga}]}$  configuration is close to the starting configuration with only a slight outward relaxation of the surrounding Ga neighbours leading to an increase in length of both  $I_{\text{Ga}}-\text{Ga}$  bond by about 7.0 %, to 2.596 Å. The volume expansion around the  $\text{tetra}_{[\text{Ga}-\text{Ga}]}$  goes down rapidly and affects only the first and second neighbor shells along the tetrahedral axes. The  $\text{tetra}_{[\text{Ga}-\text{As}]}$  configuration undergoes a similar expansion and the  $I_{\text{Ga}}-\text{As}$  bond lengths are stretched by 5.3 % from 2.425 to 2.554 Å.

Both the 110-split $_{[\text{Ga}-\text{As}]}$  and 100-split $_{[\text{Ga}-\text{Ga}]}$  are found to be metastable. The formation energies are higher:  $E'_f = 4.24$  eV for 110-split $_{[\text{Ga}-\text{As}]}$  and  $E'_f = 4.92$  eV for 100-split $_{[\text{Ga}-\text{Ga}]}$ . In addition, the stress imposed on the lattice is more important, and affects significantly the more distant neighbours.

The 100-split $_{[\text{Ga}-\text{Ga}]}$  experiences the largest lattice deformation around the defect among other interstitial defects as illustrated in Figure 1 where surrounding lattice atoms are shown. This relaxed configuration is a dumbbell formed by  $I_{\text{Ga}}$  and the displaced Ga lattice atom. The dumbbell is centered and symmetric with respect to the middle vacant lattice gallium site with each Ga atom being located at 1.10 Å apart. The length of the dumbbell shrinks by about 9.2% (from 2.42 to 2.20 Å) bringing the two atoms closer. For their part, atoms at the first and second shell neighbors experience an outward relaxation and are pushed away from their original position by about 0.46 and 0.21 Å respectively. Thus, considering both effects the bond length between each of the Ga atoms forming the dumbbell and their first As lattice neighbors increases by approximately 17.4% from 1.99 to 2.34 Å as the distance to the second nearest neighbors grows from 3.22 to 3.47 Å, a change of about 7.8%.

Finally, the 100-split $_{[\text{Ga}-\text{As}]}$  self-interstitial is highly unstable and does not converge to any stable state. For this reason, we will not attempt any further calculation using this configuration for the rest of this work.

TABLE II: Formation energies (in eV) for stable and metastable Ga interstitial configurations in GaAs for various charge states.

Stable configurations	Net system charge $q$						
	-3	-2	-1	0	+1	+2	+3
$\text{tetra}_{[\text{Ga}-\text{Ga}]}$	8.37	6.40	4.62	3.42	2.40	2.81	3.43
$\text{tetra}_{[\text{Ga}-\text{As}]}$	8.65	6.72	4.98	3.73	2.67	2.91	3.41
110-split $_{[\text{Ga}-\text{As}]}$	—	6.42	4.99	4.24	↓	↓	↓
111-split $_{[\text{Ga}-\text{As}]}$	—				3.33	3.74	4.35
100-split $_{[\text{Ga}-\text{Ga}]}$	—	7.75	6.16	4.92	3.33	4.15	4.62

In order to test the stability of the four metastable configurations found, we further relaxed them with a more accurate force threshold of 0.002 eV/Å. The observed change in geometry and formation energy is negligible indicating that our results are already well converged with the former force threshold of 0.04 eV/Å.

### B. Structural stability of charged self-interstitials

Having characterized the stability of the set of neutral initial self-interstitial configuration, we now turn to charge states. All charge configurations are also started from the eight ideal unrelaxed configurations except for the 110-split $_{[\text{Ga}-\text{As}]}$ , which could not relax in the allowed time from the ideal position and which was started in the neutral relaxed configuration instead.

For  $q = +1$  charged interstitials, the relaxation follows the same scenario as for the neutral defect for all first seven configurations of Fig. 1 (top): the overall stability order is kept unchanged and the  $\text{tetra}_{[\text{Ga}-\text{Ga}]}$  configuration is still the most stable defect. For their part, the unstable interstitial states relaxed into the same metastable configuration as in the neutral case with one exception, however: the 110-split $_{[\text{Ga}-\text{As}]}$  now relaxes into a 111-split $_{[\text{Ga}-\text{As}]}$  (Fig. 2) but keeps the same stability order with respect to the other metastable defects.

Interestingly, the resulting formation energies calculated for +1 charged defects are significantly lower than in the neutral charge state in all cases:  $\text{tetra}_{[\text{Ga}-\text{Ga}]}$  has a formation energy of  $E'_f = 2.40$  eV, followed by  $\text{tetra}_{[\text{Ga}-\text{As}]}$  with  $E'_f = 2.63$  eV, then 111-split $_{[\text{Ga}-\text{As}]}$  with  $E'_f = 3.33$  eV and finally 100-split $_{[\text{Ga}-\text{Ga}]}$  with also  $E'_f = 3.33$  eV.

The removal of an electron for  $I_{\text{Ga}}$  in GaAs stabilizes all defects uniformly with respect to their respective neutral state while the stability order of each interstitial configuration with regard to each other remains about the same. To fully characterize this effect, we have further relaxed the most stable interstitial geometries —  $\text{tetra}_{[\text{Ga}-\text{Ga}]}$ ,  $\text{tetra}_{[\text{Ga}-\text{As}]}$ , 100-split $_{[\text{Ga}-\text{Ga}]}$ , and 110 or 111 splits $_{[\text{Ga}-\text{As}]}$  — for the  $q = -1$ ,  $q = \pm 2$  and  $\pm 3$

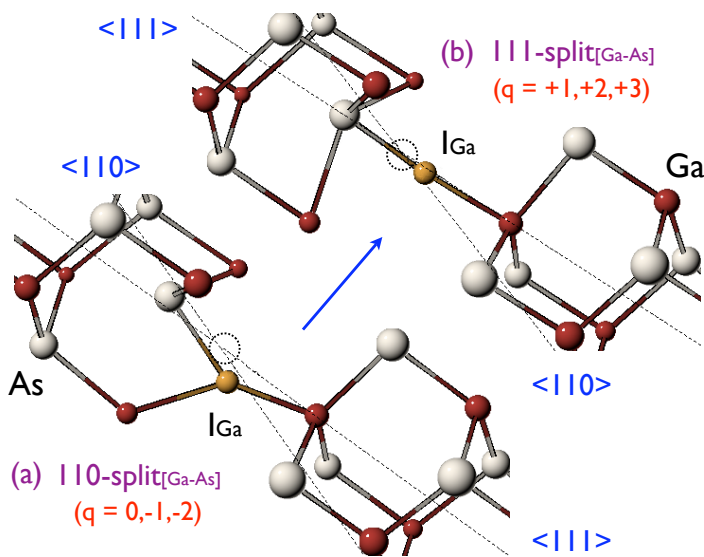


FIG. 2: (Color online) The two distinct 110 (a) and 111 (b) splits seen from a 110 view. Dash lines correspond to  $\langle 111 \rangle$  and  $\langle 110 \rangle$  crystalline axis (indicated in blue) and dotted circles refer to the regular crystalline position of the displaced arsenic atom. Gallium atoms are red while arsenics are white; the interstitial Ga atom is colored yellow. Some lattice atoms have been removed for clarity.

charges, supposing that the unstable interstitial configurations do not stabilize in these highly charged systems.

Table II shows the formation energies of the five metastable relaxed configurations in increasing order of formation energy, for seven charge states ( $q = \pm 3, \pm 2, \pm 1$ , and 0) with the associated monopole correction applied, as explained in Section II B. The missing numbers for charge  $q = -3$  correspond to configurations that did not achieve convergence even after long simulations. Additionally, starting from the neutral 110-split $_{[\text{Ga}-\text{As}]}$  configuration, relaxations towards positive charges all induce a change in the orientation of the dumbbell leading to the nearly same 111-split $_{[\text{Ga}-\text{As}]}$  (as indicated by downside arrows in Table II) while relaxations of negatively charged 110-split $_{[\text{Ga}-\text{As}]}$  preserve the initial  $\langle 110 \rangle$  orientation.

Figure 2 illustrates the shift of orientation from 110-split $_{[\text{Ga}-\text{As}]}$  for neutral and negative charges to 111-split $_{[\text{Ga}-\text{As}]}$  for positive charges. The length of the dumbbell is around 2.24 Å for 111-split $_{[\text{Ga}-\text{As}]}^{+1,+2,+3}$  and about 2.33 Å for 110-split $_{[\text{Ga}-\text{As}]}^{0,-1,-2}$ .

From Table II, we observe that the lowest formation energy for all the four interstitial configurations is associated with the +1 charged state. For a given symmetry, we see that the formation energy monotonically decreases with increasing charge, from  $-3$  to  $+1$  before going up for more positive charge states. In all cases, the formation energies for positive charges are lower than for the negative ones.

Looking at particular charged interstitials, we ob-

serve also that the order of stability between different interstitial configurations that we observe in neutral charge state is conserved under the variation of the net charge of the system (except for  $-2$  charged state where 110-split $_{[\text{Ga}-\text{As}]}$  formation energy is below that of tetra $_{[\text{Ga}-\text{As}]}$ ). Moreover, apart from higher charge states, there is a somewhat constant difference of 0.30 eV between the two different tetrahedral configurations for the same charge states from  $-3$  to  $+1$  where the formation energy reaches its minimum value.

We note also that a degeneracy appears between pairs of interstitials for two charge states: at  $+1$ , both 111 and 100 splits have about the same formation energy while at  $-1$ , the same is true for tetra $_{[\text{Ga}-\text{As}]}$  and 110-split $_{[\text{Ga}-\text{As}]}$ . This suggests that the 110 and 111 split $_{[\text{Ga}-\text{As}]}$  configurations play a key role in GaAs crystals, serving as transitional configurations when passing from tetra $_{[\text{Ga}-\text{As}]}$  at charge  $-1$  to 100-split $_{[\text{Ga}-\text{Ga}]}$  at charge  $+1$ , successively losing two electrons, one at a time (the 111-split being an intermediate step from neutral to  $+1$  charged state). As a result, this specific transition process could be an important diffusion path for impurities in GaAs crystals.

Although, for charge  $+3$ , the formation energies of both tetrahedral configurations are also near, it could be a finite size effect associated with the stress induced by the high positive net charge, introducing a bias in our calculation.

### C. Competition between $I_{\text{Ga}}$ charge states under doping conditions

We now look at the effect of doping by varying the Fermi level with the help of the parameter  $\mu_e$  in equation 3. These effects are best seen by comparing data for multiple charge states and we concentrate on the configurations of Table II. Because of the similarities in the stability diagrams of tetra $_{[\text{Ga}-\text{Ga}]}$  and tetra $_{[\text{Ga}-\text{As}]}$  only the first one is shown in Figure 3. The diagram for 100-split $_{[\text{Ga}-\text{Ga}]}$  and 110-split $_{[\text{Ga}-\text{As}]}$  are shown in Figures 4 and 5 respectively. In all figures, the Fermi level is set by reference to the valence band maximum.

Because DFT calculations are known to underestimate the band gap (the present calculation gives a band gap of 0.82 eV compared to 1.52 eV at  $T = 0$  K reported by experiment), it is common to vary the Fermi level in the window of the experimental band gap to obtain the full picture<sup>22</sup>. Note, that even if our calculated ionization levels have a conduction band character, they have not been corrected for that because the efficiency of the several band gap correction methods is system dependent and testing them is out of the scope of the present work<sup>23</sup>.

Fig. 3 shows the formation energy as a function of the doping level for the tetrahedral interstitial. Dotted lines point at the location of ionization level, identified by intersecting formation energy lines. Three stability domains, labeled by (I), (II), and (III), are found

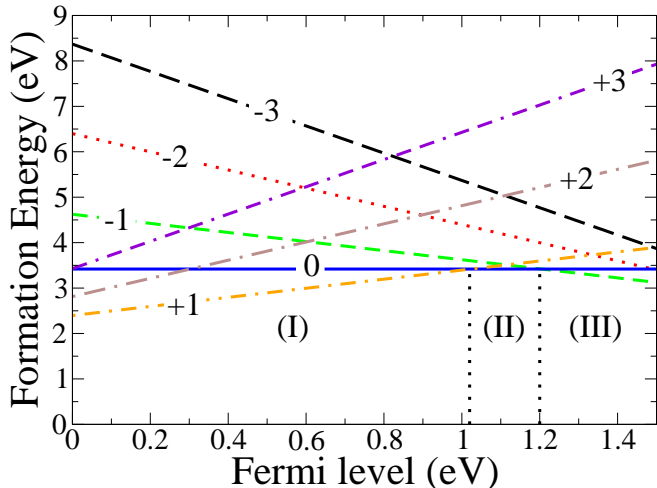


FIG. 3: (Color online) Formation energies as function of Fermi level for various charge states of the  $\text{tetra}_{[\text{Ga}-\text{Ga}]}$  configuration at 0 K. Dotted lines point at the ionization level locations delimiting the three stability domains labeled by (I), (II), and (III).

for  $\text{tetra}_{[\text{Ga}-\text{Ga}]}$  corresponding to successive dominant charge states  $+1$ ,  $0$ , and  $-1$  respectively. The same stable states occur for  $\text{tetra}_{[\text{Ga}-\text{As}]}$ , with almost the same ionization energies. Table III summarizes these ionization energies, calculated from equation 6.

The  $100\text{-split}_{[\text{Ga}-\text{Ga}]}$  exhibits a different behavior as the line of charge state  $q = -1$  crosses the line from the state  $q = +1$  *before* the horizontal neutral  $q = 0$  state line (about 0.18 eV below) allowing a direct transition between  $q = -1$  and  $+1$ , in a so-called *negative-U* effect. Only two stability domains labeled by (I) and (II) are found, for charge  $+1$  and  $-1$  respectively (see Fig. 4). This effect might not exist in real systems since region II occurs at the edge of the conduction band. Any fluctuation or error might therefore screen region II. The reverse could be true for the tetrahedral interstitials (Fig. 3). In this figure, region II is very narrow, set in the middle of the gap, and a fluctuation could remove it altogether, this time inducing a negative-U effect.

We note also that the transition domain of the  $100\text{-split}$  occurs just below the minimum of the conduction band, meaning that it is only accessible in extreme doping condition. For most purposes, the domain of charge  $+1$  will be the only one that matters.

Another negative-U effect causes the transition from  $111\text{-split}_{[\text{Ga}-\text{As}]}^{+1}$  to  $110\text{-split}_{[\text{Ga}-\text{As}]}^{-1}$  (Fig. 5). Once again, the transition occurs very near to the neutral charge state line, only 0.07 eV below. Here, however, the transition is located at midgap and should therefore play a more important role. Moreover, as this  $(+1/-1)$  negative-U transition manifests itself by a change in the

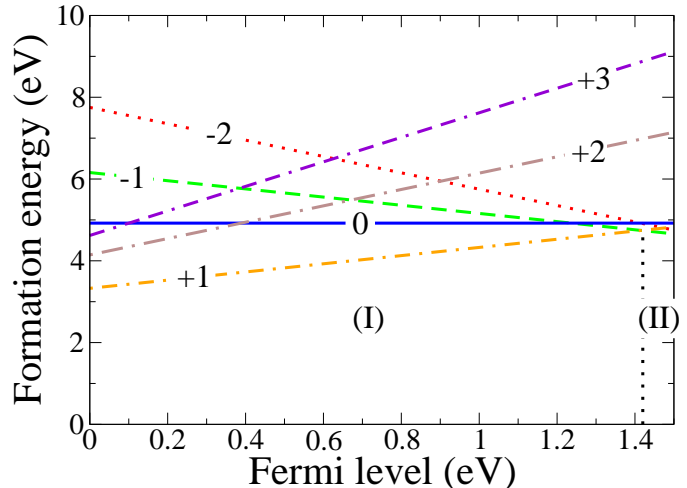


FIG. 4: (Color online) Formation energies as function of Fermi levels for various charge states of the  $100\text{-split}_{[\text{Ga}-\text{Ga}]}$  configuration at 0 K.

TABLE III: Ionization energies of metastable  $I_{\text{Ga}}$  configurations in GaAs (see equation 6). Negative-U transition  $(+1/-1)$  for  $\text{split}_{[\text{Ga}-\text{As}]}$  changes the dumbbell orientation from 111 to 110.

Configurations	Ionization levels (eV)			
	$+1/0$	$0/-1$	<i>Negative-U</i>	
$\text{tetra}_{[\text{Ga}-\text{Ga}]}$	1.02	1.20		
$\text{tetra}_{[\text{Ga}-\text{As}]}$	1.06	1.25		
$100\text{-split}_{[\text{Ga}-\text{Ga}]}$			1.42	
$110 \& 111 \text{ splits}_{[\text{Ga}-\text{As}]}$			0.83	1.42

orientation of the dumbbell from 111 to 110, it should therefore be relatively insensitive to the various limitations of the current simulation and other possible thermal fluctuations.

Similarly to the  $100\text{-split}$ , we find also a transition (here,  $-1/-2$ ) for  $110\text{-split}_{[\text{Ga}-\text{As}]}$  near the conduction band minimum. Since this transition level has itself a conduction band character its position might be affected by the DFT-bandgap underestimation and must be treated with care. Although we did not manage to converge the  $110\text{-split}_{[\text{Ga}-\text{As}]}^{-3}$ , it is interesting to note that if the trend for the negative charges seen in Fig. 5 holds, we should see a negative-U transition between charge  $-1$  and  $-3$  before the  $-1/-2$  transition for this charge.

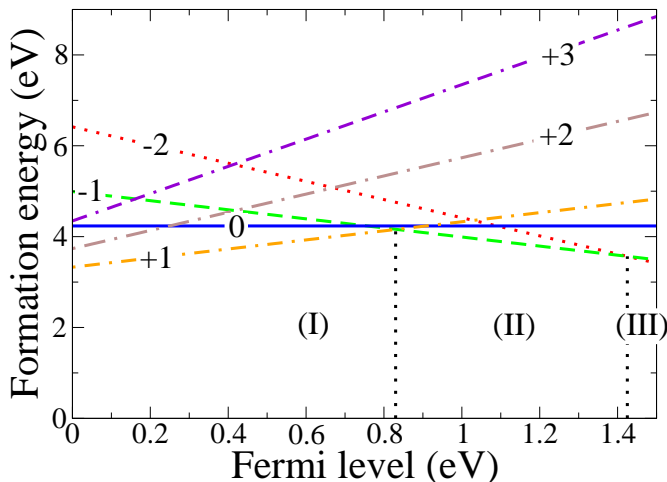


FIG. 5: (Color online) Formation energies as function of Fermi levels for various charge states of the 110 ( $q = -2, -1, 0$ ) and 111 ( $q = +1, +2, +3$ )  $\text{split}_{[\text{Ga-As}]}$  configuration at 0 K.

## V. DISCUSSION

Here we discuss and compare our results with previous *ab initio* and tight-binding calculations<sup>13,14,18,21</sup>, as well as with recent experimental data from Bracht<sup>1</sup>. While it was not clearly indicated in most of the theoretical works, whether the *tetrahedral* interstitial label meant  $\text{tetra}_{[\text{Ga-As}]}$  or  $\text{tetra}_{[\text{Ga-Ga}]}$ , we will presume that it refers to the former.

Chadi<sup>21</sup> was first to report self-interstitial configurations and energetics using self-consistent pseudopotential relaxations on GaAs supercells with 32+1 atoms. Almost the same set of starting configurations as in the present work was studied under different charging, but the resulting stability order was completely different from our. Indeed, Chadi found the bond-center (*twofold*) configurations to be the most stable configuration for  $q = +1$  and the 110- $\text{split}_{[\text{Ga-As}]}$  for  $q = 0, -1$ . The  $\text{tetra}_{[\text{Ga-As}]}$  was found to have the lowest formation energy only under +2 charging. The difference between this work and ours is mostly due to the strong finite size effects present in a 32+1 unit cell.

For their part, Zollo and Nieminen<sup>13</sup> studied the full set of interstitial positions — except for  $\text{tetra}_{[\text{Ga-Ga}]}$  — in a 64+1 atomic supercell and for the neutral state only. They found that the hexagonal, bond-center, and 100-splits are unstable, converging to the tetrahedral interstitial position. They also identified the  $\text{tetra}_{[\text{Ga-As}]}$ , the 110- $\text{split}_{[\text{Ga-Ga}]}$ , and the 110- $\text{split}_{[\text{Ga-As}]}$  to be metastable, with increasing formation energy. Recently, Volpe *et al.*<sup>14</sup> used a large supercell of 216+1 atoms with tight binding method to study  $I_{\text{Ga}}$  in GaAs, again treating exclusively the neutral charge state and com-

puting formation energies relative to the tetrahedral interstitial formation energy only. The metastable structures identified at the neutral state were classified in increasing order of formation energy: the  $\text{tetra}_{[\text{Ga-As}]}$ , then the 110- $\text{split}_{[\text{Ga-Ga}]}$ , the 110- $\text{split}_{[\text{Ga-As}]}$ , and the 100- $\text{split}_{[\text{Ga-Ga}]}$ . As was shown in Tab. II, our results show that 100- $\text{split}_{[\text{Ga-Ga}]}$  is indeed metastable as found by Volpe *et al.* They disagree with both Zollo and Nieminen and Volpe *et al.* with respect to the 110- $\text{split}_{[\text{Ga-Ga}]}$  interstitial, however, which becomes unstable and prefers to relax to  $\text{tetra}_{[\text{Ga-As}]}$  according to our 216 DFT calculations.

The difference between these calculations and the one presented here are caused by (1) size effect associated self-interactions of the defects in unit cells that are too small and (2) the accuracy of the potential (DFT versus tight-binding), particularly when important structural changes are taking place, as is the case for split interstitials, for example.

Focusing on the dominant charge state of  $I_{\text{Ga}}$  in GaAs, the results of Section IV show that higher charge states ( $q = \pm 2, \pm 3$ ) are not relevant and should contribute negligibly to the total experimental self-diffusion profiles. This agrees well with recent experimental results from Bracht<sup>1</sup> that identified  $I_{\text{Ga}}^0$  and  $I_{\text{Ga}}^{+1}$  as important species for diffusion process in GaAs crystals doped with Zn (but with lower contribution than vacancies). Our results provide a strong support for the picture proposed by Bracht, disproving earlier models which generally predict diffusion process controlled mainly by +2 and +3 interstitials. In particular, our calculations show that +2 and +3 charge states exhibit higher formation energies than the +1 charge defect, contrary to what was found by Zhang and Northrup<sup>2</sup>. Using a 32+1 atoms supercell within DFT-LDA, these authors identified the dominant native defect to be the  $\text{tetra}_{[\text{Ga-As}]}^{+3}$  in Ga-rich condition under p-type doping. Similarly, more accurate *ab-initio* calculation of Zollo *et al.*<sup>18</sup> find negative-U effects for  $\text{tetra}_{[\text{Ga-As}]}$  with (+3/+1) and (+1/-1) ionization levels located at 0.29 and 1.23 eV above the VBM respectively, still giving an important role to the triply positive state which we do not see.

Again, size effects can explain many of these divergences. For example, finite size effects have been reported recently by Schick *et al.*<sup>24</sup> for As 110-split interstitials in GaAs. While a 65 supercell calculation with a  $2 \times 2 \times 2$  k-points mesh predict the stability of +2 charge state starting for the VBM. This charge state disappears completely from the diagram as soon as a supercell as large as 217 is used with different k-point meshes leaving the +1 charge state as the most stable near VBM.

Qualitatively, the formation energies for  $\text{tetra}_{[\text{Ga-Ga}]}$  in stoichiometric GaAs ( $\Delta\mu = 0$ ) we compute depend on doping conditions:  $E_f(I_{\text{Ga}}^0) = 3.42$  eV,  $E_f(I_{\text{Ga}}^{+1}) = 2.4$  to 3.92 eV,  $E_f(I_{\text{Ga}}^{+2}) = 2.81$  to 4.33 eV, and for  $E_f(I_{\text{Ga}}^{+3}) = 3.43$  to 4.95 eV. All these values remain in the window of allowed values compared to the activation enthalpy ( $H_a$ ) obtained after fitting the experimen-

tal profiles.  $H_a$  for  $I_{Ga}^{0,+1}$ -mediated Ga diffusion in GaAs reported by Bracht<sup>1</sup> was  $5.45 \pm 0.12$  and  $5.80 \pm 0.32$  eV for neutral and +1 charge states respectively. Since we do not know the migration enthalpies of  $I_{Ga}$  in GaAs with respect to the charge state, it is not possible at this point to push further and identify the charge state responsible for the Zn diffusion profiles. Only a detailed study of the migration mechanisms of  $I_{Ga}$  in GaAs similar to the one performed recently for  $V_{Ga}$  in GaAs as function of the charge state<sup>25</sup> can give the answer to this question.

## VI. CONCLUSIONS

In this work, we have studied the stability of Ga self-interstitial for multiple charge states ( $q = 0, \pm 1, \pm 2, \text{ and } \pm 3$ ) within DFT-LDA using the local-orbital basis set program SIESTA at  $T = 0$  K. Out of the eight initial configurations tested, five were found to be metastable after full relaxation. As a general rule, the most stable configuration is found to be  $\text{tetra}_{[\text{Ga}-\text{Ga}]}$  for all charge states, in addition positively charged interstitials are more stable than negative ones for all tested charges and configurations.

After studying the competition between various configuration and charges of  $I_{Ga}$ , we conclude that predominant gallium interstitials in GaAs are charged +1, neutral or at most -1 depending on doping conditions. This agrees well with the recent conclusions driven by Bracht *et al.* which states that fits of recent as well as earlier diffusivity profiles in Zn doped GaAs are more accurate if the role  $I_{Ga}^{+1,0}$  is considered. At low temperatures, when the formation energy dominates,  $I_{Ga}$  prefers to occupy the tetrahedral interstitial configuration being surrounded by gallium atoms ( $\text{tetra}_{[\text{Ga}-\text{Ga}]}$ ). The competition between  $\text{tetra}_{[\text{Ga}-\text{Ga}]}$  and the other metastable configuration increases as we approach the experimental

processing temperatures (above 1000 K) but not sufficiently to invert the order of stability. For example under P-type doping at 1000 K, the  $\text{tetra}_{[\text{Ga}-\text{Ga}]}^{+1}$  still has a probability of occurrence about 100 times larger than  $I_{Ga}^{+1}$  and  $10^5$  times larger than the 110 and 100-split interstitials.

The comparison of our results with previous works show also that size of the simulation supercell can affect significantly the stability and formation energy of  $I_{Ga}$ , and both tight-binding and *ab-initio* calculations become more reliable with increasing cell size. The size of the supercell affects the charge state of the dominant defect and modifies also the metastability of other defects such as the split interstitials. In this case, the use of a 216+1 atoms supercell allows us to observe for the first time a change in the orientation of the split from  $\langle 110 \rangle$  to  $\langle 111 \rangle$  after the removal of one electron from the neutral configuration.

In spite of the excellent agreement with recent experimental results, further calculations, including the entropic contributions and the diffusion pathways, are still necessary to obtain a complete picture of the role of  $I_{Ga}$  and reveal the possible importance of other charge states and configurations.

## VII. ACKNOWLEDGMENTS

We would like to thank Dr. Giuseppe Zollo for sharing his results on bulk As, Ga, and GaAs chemical potentials. Dr. Harmurt Bracht for fruitful discussion. This work is funded in part by NSERC (Canada), FQRNT (Québec) and the Canada Research Chair Foundation. All the simulations were run with the computer network support of Réseau québécois de calcul et de haute performance (RQCHP) which is greatly appreciated.

\* Electronic address: marc.andre.malouin@umontreal.ca

† Electronic address: f.el.mellouhi@umontreal.ca

‡ Electronic address: Normand.Mousseau@umontreal.ca

<sup>1</sup> H. Bracht and S. Brotzmann, Phys. Rev. B **71**, 115216 (2005).

<sup>2</sup> S. B. Zhang and J. E. Northrup, Phys. Rev. Lett. **67**, 2339 (1991).

<sup>3</sup> R. Jansen, D. S. Wolde-Kidane, and O. F. Sankey, J. Appl. Phys. **64**, 2415 (1988).

<sup>4</sup> M. D. Deal and H. G. Robinson, Solid-State Electron **33**, 665 (1989).

<sup>5</sup> R. Mosca, P. Bussei, S. Franchi, P. Frigeri, E. Gombia, A. Carnera, and M. Peroni, J. Appl. Phys. **93**, 9709 (2003).

<sup>6</sup> J. C. Hu, M. Deal, and J. D. a. Plummer, J. Appl. Phys. **78**, 1595 (1995).

<sup>7</sup> J. C. Hu, M. Deal, and J. D. a. Plummer, J. Appl. Phys. **78**, 1606 (1995).

<sup>8</sup> S. Yu, T. Y. Tan, and U. Gösele, J. Appl. Phys. **69**, 3547 (1991).

<sup>9</sup> M. Uematsu, K. Wada, and U. Gösele, Appl. Phys. A **55**, 301 (1991).

<sup>10</sup> E. P. Zucker, A. Hashimoto, T. Fukunaga, and N. Watanabe, Appl. Phys. Lett. **54**, 564 (1989).

<sup>11</sup> H. P. Winteler, Helv. Phys. Acta **44**, 451 (1971).

<sup>12</sup> G. Bösker, N. A. Stolwijk, H.-G. Hettwer, A. Rucki, W. Jäger, and U. Södervall, Phys. Rev. B **52**, 11927 (1995).

<sup>13</sup> G. Zollo and R. M. Nieminen, J. Phys. Condens. Matter **15**, 843 (2003).

<sup>14</sup> M. Volpe, G. Zollo, and L. Colombo, Phys. Rev. B **71**, 075207 (2005).

<sup>15</sup> D. Sánchez-Portal, P. Ordejón, E. Artacho, and J. M. Soler, Int. J. Quant. Chem. **65**, 453 (1997).

<sup>16</sup> J. M. Soler, E. Artacho, J. Gale, A. García, J. Junquera, and P. Ordejón, J. Phys. Condens. Matter **14**, 2745 (2002).

<sup>17</sup> F. El-Mellouhi and N. Mousseau, Phys. Rev. B **71**, 125207 (2005).

<sup>18</sup> G. Zollo, Y. J. Lee, and R. M. Nieminen, J. Phys. Condens. Matter **16**, 8991 (2004).



- <sup>19</sup> D. R. Lide, ed., *Handbook of Chemistry and Physics* (CRC, Boca Raton, FL, 2003), 83rd ed.
- <sup>20</sup> G. Makov and M. C. Payne, Phys. Rev. B **51**, 4014 (1995).
- <sup>21</sup> D. J. Chadi, Phys. Rev. B **46**, 9400 (1992).
- <sup>22</sup> C. G. Van de Walle and J. Neugebauer, J. Appl. Phys. **95**, 3851 (2004).
- <sup>23</sup> C. W. M. Castleton, A. Höglund, and S. Mirbt, Phys. Rev. B **73**, 035215 (2006).
- <sup>24</sup> J. T. Schick, C. G. Morgan, and P. Papoulias, Phys. Rev. B **66**, 195302 (2002).
- <sup>25</sup> F. El-Mellouhi and N. Mousseau, Phys. Rev. B **74**, 205207 (2006).